Eddy-viscosity vs. Second-Order Closures for Flows in Noncircular Ducts

Bassam A. Younis and Davor Cokjat
Dept. of Civil Engineering, City University, London EC1V 0HB, U.K.

This article deals with prediction of turbulent flows in ducts of noncircular cross sections and, in particular, assessment of the performance in such flows of two very different models of turbulence. One model is of the two-equation, eddy-viscosity type, which is used in conjunction with a non-linear stress-strain relationship. The other is a complete Reynolds-stress transport closure that involves the solution of a differential transport equation for each of the six components of the Reynolds-stress tensor. The flows considered are characterized by the presence of secondary motions that are largely driven by the turbulence anisotropy and whose prediction remains a severe challenge to turbulence closures. Data from several experiments involving such flows are used here to assess the overall performance of the two models. It is found that the two models yield very similar results that are also of adequate engineering accuracy — an outcome that argues in favor of the use of the nonlinear two-equation model in practical computations.

Introduction

Turbulent flows in noncircular ducts arise in a wide range of applications in the process and nuclear industries, and hence the need for a reliable and economical method for predicting their behavior. An important feature of these flows, and one that must be catered to in the simulations method, is the presence in such flows of secondary motions in planes normal to the main-flow direction. The mechanism for the generation of these motions is well understood: it arises from the anisotropy of the turbulence field and from gradients of the Reynolds shear stresses, both contributing to the generation of streamwise vorticity (see, e.g., Brundrett and Baines, 1964). The turbulence models that are commonly used in industry (e.g., the two-equation, $k-\epsilon$ model) have proved inadequate for the present purposes. This is so because they are based on Boussinesq's eddy-viscosity concept in which the Reynolds stresses are assumed to be linearly proportional to the local mean rates of strain. It is easily shown that, with this assumption, and for fully-developed flow conditions, the turbulence field is predicted to be isotropic, and consequently no turbulence-driven motions are produced. Since the problem lies in the form of the assumed stress-strain relation, it appears sensible to seek to extend the applicability of such widely-used closures by abandoning Boussinesq's *linear* relationship in favor of a more general form. Several alternative forms have been reported in the literature. Lumley (1970), for example, proposed a generalized constitutive relationship arrived at by identifying the appropriate scaling parameters that enter into the relation, and then expressing it as a finite tensor polynomial. Pope (1975) pointed out that Lumley had made "illicit use" of the alternating tensor density and that rendered the results invalid. Pope then proposed an alternative, explicit and frame-indifferent relation for the Reynolds stresses, but remarked that the three-dimensional expression was "so intractable as to be of no value." Speziale (1987) proposed another alternative in which the Reynolds stresses were made a *quadratic* function of the mean rates of strain. Younis and Abdellatif (1989) utilized this last proposal in a study of the effects of turbulence-driven secondary motions on the bed-load sediment transport in ducts and obtained good correlations with the measured boundary shear-stress distributions. In this study, we conduct a systematic assessment of Speziale's model using data from a wide range of flows in noncircular ducts.

In order to put the nonlinear model's performance in a proper perspective, comparisons are made with results from an alternative closure strategy. The traditional route for predicting flows in noncircular ducts has been to invoke the assumption of local equilibrium in order to reduce the differen-

Correspondence concerning this article should be addressed to B. A. Younis.

tial equations governing the transport of the Reynolds stresses into algebraic approximations (Nakayama et al., 1983; Demuren and Rodi, 1984). We have not adopted this approach here as the resulting *Algebraic Stress Model* equations are implicit in the Reynolds stresses and this can sometimes complicate their solution. Such models are also not always strictly frame-indifferent, and this limits their usefulness to flows that can be analyzed with the Cartesian coordinate system. Instead, we have obtained comparative results by using a complete Reynolds-stress transport closure based on the solution of the differential transport equations for each of the six components of the Reynolds-stress tensor together with an equation for the isotropic dissipation rate. In this article we describe a novel extension of this model to capture the correct level of turbulence anisotropy in confined ducts and give details of the model's implementation in a three-dimensional finite-volume code.

The Turbulence Models

For steady, fully developed constant-property flow in a straight duct, the equations describing the conservation of mass and momentum are given as (see Figure 1 for notation):

$$\frac{\partial U}{\partial x}+\frac{\partial V}{\partial y}=0 \tag{1}$$

$$U\frac{\partial U}{\partial x}+V\frac{\partial U}{\partial y}=\frac{\partial}{\partial x}\left(\nu\frac{\partial U}{\partial x}-\overline{u^2}\right)+\frac{\partial}{\partial y}\left(\nu\frac{\partial U}{\partial y}-\overline{uv}\right)-\frac{1}{\rho}\frac{\partial p}{\partial x} \tag{2}$$

$$U\frac{\partial V}{\partial x}+V\frac{\partial V}{\partial y}=\frac{\partial}{\partial x}\left(\nu\frac{\partial V}{\partial x}-\overline{uv}\right)+\frac{\partial}{\partial y}\left(\nu\frac{\partial V}{\partial y}-\overline{v^2}\right)-\frac{1}{\rho}\frac{\partial p}{\partial y} \tag{3}$$

$$U\frac{\partial W}{\partial x}+V\frac{\partial W}{\partial y}=\frac{\partial}{\partial x}\left(\nu\frac{\partial W}{\partial x}-\overline{uw}\right)+\frac{\partial}{\partial y}\left(\nu\frac{\partial W}{\partial y}-\overline{vw}\right)-\frac{1}{\rho}\frac{\overline{\partial p}}{\partial z}. \tag{4}$$

In the preceding equations, U and V are the components of the secondary motion and W is the velocity in the streamwise (z) direction. All terms involving the streamwise gradients $\partial/\partial z$ (bar for the mean pressure) have been neglected in accordance with the fully developed flow assumption. Note that the pressure field has been split into a cross-sectional averaged component ($\overline{p(z)}$), that drives the streamwise velocity and perturbations on this quantity ($p(x,y)$), which arise from the secondary motions. This practice was first suggested by Patankar and Spalding (1972) and has profound implications on the method of solving these equations, as will be explained later.

The unknown Reynolds-stresses in Eqs. 2–4 are obtained by one of the following two alternatives.

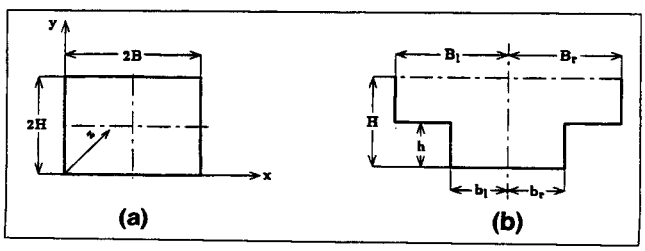

Figure 1. Duct-flow notation.

(a) Rectangular duct: $AR = B/H$; (b) Compound duct: $h^* = (H-h)/H$; $AR = (B_l + B_r)/2H$.

Nonlinear $k-\epsilon$ model

Speziale's (1987) proposal for the Reynolds stresses is given (in standard Cartesian tensor notation) as:

$$-\overline{u_iu_j}=-\frac{2}{3}\delta_{ij}k+2\nu_t\overline{D_{ij}}+C_EL\left(\overline{D_{im}}\,\overline{D_{mj}}-\frac{1}{3}\overline{D_{mn}}\,\overline{D_{mn}}\delta_{ij}\right)+C_EL\left(\overline{\overset{\circ}{D}_{ij}}-\frac{1}{3}\overline{\overset{\circ}{D}_{mm}}\delta_{ij}\right). \tag{5}$$

In Eq. 5, $\overline{D_{ij}}$ is the mean rate of strain tensor:

$$\overline{D_{ij}}=\frac{1}{2}\left(\frac{\partial U_i}{\partial x_j}+\frac{\partial U_j}{\partial x_i}\right), \tag{6}$$

$\overline{\overset{\circ}{D}_{ij}}$ is the Oldroyd derivative, defined as:

$$\overline{\overset{\circ}{D}_{ij}}=\frac{\partial\overline{D_{ij}}}{\partial t}+U_m\frac{\partial\overline{D_{ij}}}{\partial x_m}-\frac{\partial U_i}{\partial x_m}\overline{D_{mj}}-\frac{\partial U_j}{\partial x_j}\overline{D_{mi}}, \tag{7}$$

and L is the turbulence length scale, given by

$$L=4C_\nu^2\frac{k^3}{\epsilon^2}. \tag{8}$$

The top line in Eq. 5 corresponds to Boussinesq's linear relationship, the two lines below it introduce the extra terms that are quadratic in the mean rates of strain. The latter arise both from the multiplication of strain rates with other strain rates and from the presence of the Oldroyd derivative, which involves spatial and temporal transport of the mean strain rates. The model, when expanded in full, is quite lengthy, but can nevertheless be implemented in a compact form in standard simulation methods by recognizing the rotational symmetries involved.

The complete model requires the solution of a differential transport equation for the turbulence kinetic energy (k) and another for its rate of dissipation by viscous action (ϵ). These are given as

$$U_j\frac{\partial k}{\partial x_j}=\frac{\partial}{\partial x_j}\left(\frac{\nu_t}{\sigma_k}\frac{\partial k}{\partial x_j}\right)+P_k-\epsilon \tag{9}$$

Table 1. Coefficients of Speziale's Nonlinear $k-\epsilon$ Model

C_μ	σ_k	σ_ϵ	$C_{\epsilon 1}$	$C_{\epsilon 2}$	C_E
0.09	1.0	1.22	1.44	1.92	1.68

$$U_j \frac{\partial \epsilon}{\partial x_j} = \frac{\partial}{\partial x_j}\left(\frac{\nu_t}{\sigma_\epsilon}\frac{\partial \epsilon}{\partial x_j}\right) + \frac{\epsilon}{k}(C_{\epsilon_1} P_k - C_{\epsilon 2}\epsilon). \quad (10)$$

Speziale's model involves a single new coefficient (C_E), evaluated by the originator with reference to data from the fully-developed pipe flow. The value of this constant, together with those of the standard $k-\epsilon$ model used in this study, are given in Table 1.

Reynolds-stress-transport closure

In this model, the unknown Reynolds stresses were obtained from the solution of differential transport equations of the form

$$\overbrace{U_k \frac{\partial \overline{u_i u_j}}{\partial x_k}}^{\text{convection}} = \overbrace{-\left(\overline{u_i u_k}\frac{\partial U_j}{\partial x_k} + \overline{u_j u_k}\frac{\partial U_i}{\partial x_k}\right)}^{\text{production}} \overbrace{-\frac{\partial}{\partial x_k}\left[\overline{u_i u_j u_k} + \frac{1}{\rho}\left(\overline{p' u_i}\delta_{jk} + \overline{p' u_j}\delta_{ik}\right) - \nu\frac{\partial \overline{u_i u_j}}{\partial x_k}\right]}^{\text{diffusion}} \underbrace{-2\nu\left(\overline{\frac{\partial u_i}{\partial x_k}\frac{\partial u_j}{\partial x_k}}\right)}_{\text{dissipation}} + \underbrace{\overline{\frac{p'}{\rho}\left(\frac{\partial u_i}{\partial x_j} + \frac{\partial u_j}{\partial x_i}\right)}}_{\text{redistribution}}. \quad (11)$$

The terms that represent "diffusion," "dissipation," and "redistribution" introduce additional unknown correlations that must now be determined. In common with standard practice, only diffusion by turbulent velocity correlation is retained and is modeled here following Daly and Harlow's (1970) gradient-transport hypothesis. Thus,

$$-\overline{u_i u_j u_k} = C_s \frac{k}{\epsilon}\overline{u_k u_l}\frac{\partial \overline{u_i u_j}}{\partial x_l}. \quad (12)$$

With the assumption of isotropic dissipative motions at high turbulence Reynolds numbers (Rotta, 1951), the dissipation term can be expressed as

$$2\nu\left(\overline{\frac{\partial u_i}{\partial x_k}\frac{\partial u_j}{\partial x_k}}\right) = \frac{2}{3}\delta_{ij}\epsilon. \quad (13)$$

The isotropic dissipation rate ϵ is obtained in this model from the solution of an equation that differs from its two-equation counterpart only by the use of a Daly and Harlow-type model for diffusion, viz.,

$$U_j \frac{\partial \epsilon}{\partial x_j} = \frac{\partial}{\partial x_k}\left(C_\epsilon \frac{k}{\epsilon}\overline{u_k u_l}\frac{\partial \epsilon}{\partial x_l}\right) + \frac{\epsilon}{k}(C_{\epsilon 1} P_k - C_{\epsilon 2}\epsilon). \quad (14)$$

The "redistribution" term is assumed to consist of three separate contributions; thus,

$$\overline{\frac{p'}{\rho}\left(\frac{\partial u_i}{\partial x_j} + \frac{\partial u_j}{\partial x_i}\right)} = \Phi_{ij,1} + \Phi_{ij,2} + \Phi_{ij,w}. \quad (15)$$

The separate elements represent, respectively, purely turbulent interactions, interactions between the mean strain field and fluctuating velocities, and, finally, corrections needed to account for the damping effects of a solid wall on the fluctuating pressure field in its vicinity.

The model adopted for $\Phi_{ij,1}$ is that of Rotta (1951), which makes it proportional to turbulence anisotropy; thus,

$$\Phi_{ij,1} = -C_1\epsilon\left(\frac{\overline{u_i u_j}}{k} - \frac{2}{3}\delta_{ij}\right). \quad (16)$$

Launder et al. (1975) proposed the following model for $\Phi_{ij,2}$:

$$\Phi_{ij,2} = -\frac{C_2+8}{11}\left(P_{ij} - \frac{2}{3}\delta_{ij}P_k\right) - \frac{30C_2-2}{55}k\left(\frac{\partial U_i}{\partial x_j} + \frac{\partial U_j}{\partial x_i}\right) - \frac{8C_2-2}{11}\left(D_{ij} - \frac{2}{3}\delta_{ij}P_k\right), \quad (17)$$

where

$$D_{ij} = -\left(\overline{u_i u_k}\frac{\partial U_k}{\partial x_j} + \overline{u_j u_k}\frac{\partial U_k}{\partial x_i}\right)$$

Launder et al. (1975) also proposed a model for $\Phi_{ij,w}$, but that was not used here. Instead, we apply separate corrections to the rapid and the return-to-isotropy parts; thus,

$$\Phi_{ij,w} = \Phi'_{ij,1} + \Phi'_{ij,2}, \quad (18)$$

and adopt the proposals of Shir (1973) and of Gibson and Launder (1978) for $\Phi_{ij,1}$ and $\Phi_{ij,2}$, respectively:

$$\Phi'_{ij,1} = C'_1\frac{\epsilon}{k}\left(\overline{u_k u_m}n_k n_m\delta_{ij} - \frac{3}{2}\overline{u_k u_i}n_k n_j - \frac{3}{2}\overline{u_k u_j}n_k n_i\right) f\left(\frac{L}{n_i r_i}\right) \quad (19)$$

$$\Phi'_{ij,2} = C'_2\left(\Phi_{km,2}n_k n_m\delta_{ij} - \frac{3}{2}\Phi_{ki,2}n_k n_j - \frac{3}{2}\Phi_{kj,2}n_k n_i\right) f\left(\frac{L}{n_i r_i}\right). \quad (20)$$

This combination of $\Phi_{ij,2}$ and $\Phi_{ij,w}$ was previously used by Younis (1982) for predicting a number of two-dimensional boundary-layer flows where it was found to perform quite well. In that study, the coefficients C'_1 and C'_2 were set equal to 0.5 and 0.1, respectively. These values were deter-

mined by reference to data for the relative stress levels in equilibrium wall flow.

The function f in the preceding equations is defined as the ratio of a typical turbulent eddy size (L) to the normal distance to a wall (n). It is assumed to vary quadratically with n and is applied to each wall independently from the other; thus,

$$f_x = \frac{L_x^2}{\langle x \rangle^2}; \qquad f_y = \frac{L_y^2}{\langle y \rangle^2}. \tag{21}$$

In the preceding equation, the turbulence length scales are evaluated from:

$$L_x = \frac{1}{\kappa} \left| \frac{\overline{uw}}{k} \right|_{wall}^{3/2} \frac{k^{3/2}}{\epsilon} \tag{22}$$

$$L_y = \frac{1}{\kappa} \left| \frac{\overline{vw}}{k} \right|_{wall}^{3/2} \frac{k^{3/2}}{\epsilon}. \tag{23}$$

The complete model contains a number of coefficients that were here assigned their standard values (e.g., Demuren and Rodi, 1984; Younis, 1982):

Solution Procedure

The solution procedure adopted here is of the finite volume variety, based on a term-by-term integration of the governing equations over cells subdividing the solution domain (Younis and Abdellatif, 1989). Certain assumptions are required in performing these integrations and in the present work we adopted the proposals of Patankar (1980) (the Power-Law Differencing Scheme) for the diffusion and convection terms. The numerical treatment takes into account the fact that the present flows are parabolic in the streamwise direction, such that influences at a particular location are not felt upstream of it, but are elliptical in cross-stream planes. The treatment is further simplified by focusing on flows that are fully developed in the streamwise direction. All the experimental data that are suited for model validation are also taken in the fully developed regime, and hence no loss of accuracy is involved. With this assumption, all terms involving streamwise gradients were dropped and integration of the governing equations was conducted in iterations (rather than physical) space. Thus, starting from assumed mean velocity and turbulence distributions, the cross-flow momentum equations were first solved and then corrected to satisfy local continuity. The streamwise momentum equation was solved next and again corrected to satisfy overall mass-flow constraints (Patankar and Spalding, 1972). Finally, the turbulence quantities were solved for sequentially using the latest available mean flow field. This process was then repeated till the normalized absolute sum of the residuals of all equations fell below 10^{-4}. In a typical simulation, this level of convergence was attained after about 3,000 iterations, which took, for the Reynolds-stress and the nonlinear models, 50 and 36 CPU minutes, respectively, to complete on a SUNSPARC 10 Workstation.

Boundary conditions are required at the walls, and these were obtained by using "wall functions," where it is assumed that the flow, at the node closest to the wall obeys the standard logarithmic distribution. This is a justifiable assumption for the present flows since the secondary motions are quite weak compared to the mean flow, and so departures from the standard log-law due to flow three-dimensionality are negligible. Local equilibrium was assumed, and hence dissipation at that node was set equal to the rate of energy production there. When the $k-\epsilon$ model was used, the value of k at the node nearest to the wall was set equal to 3.33 times the wall shear stress value. When the Reynolds-stress model was used, the values of all components of the Reynolds-stress tensor were calculated for the near-wall node by assuming that their normal gradients at the wall were zero (Younis, 1984). This practice of solving for the Reynolds stresses is less restrictive than the alternative of fixing their values and is also consistent with the assumption of a Couette-flow region close to the wall.

Table 2. Coefficients for the Reynolds-stress Closure

Constant	C_1	C_2	C_1'	C_2'	C_s	C_ϵ	$C_{\epsilon 1}$	$C_{\epsilon 2}$
	1.5	0.4	0.5	0.1	0.22	0.18	1.45	1.90

The velocity gradients that enter into the sources of the Reynolds stresses were evaluated at the near-wall nodes from the log-law relationships where appropriate, for example,

$$\frac{\partial W}{\partial y} = \frac{W\tau}{\kappa y}. \tag{24}$$

The velocity gradients that appear in the Oldroyd derivatives were also evaluated using the log-law, a practice we found necessary to obain stable solutions when using the nonlinear model.

Since only symmetric ducts are considered, only one-half of the duct was simulated and zero-gradient boundary conditions were imposed at the symmetry plane for all the variables except for the two shear-stress components $\overline{uw}$ and $\overline{uv}$, which were themselves set equal to zero.

Results and Discussion

First we consider the flow in a square-sectioned duct and, in particular, the data of Brundrett and Baines (1964) for $Re = 8.3 \times 10^4$. The solution domain consisted of only one-quarter of the duct's cross section. The computations were performed on a number of different grids, the finest of which (consisting of 22×22 unevenly distributed nodes) yielded results that were sensibly free of grid effects. Figure 2 compares the predicted and measured secondary-velocity vectors. Both reveal the existence of a total of eight cells whose distribution is symmetric about the wall and corner bisector. A quantitative comparison is shown in Figure 3 where the predictions of the secondary-flow streamlines are compared with the data of Gessner and Jones (1965), obtained at $Re = 1.5 \times 10^5$. The sense of rotation in these cells is such that slow-moving fluid from the boundary layers that develop on the side wall is convected into the core while fast-moving fluid from that region is transported toward the corners. The consequence on the contours of streamwise velocity is clear from Figure 4. These contours appear to be deflected inwards along

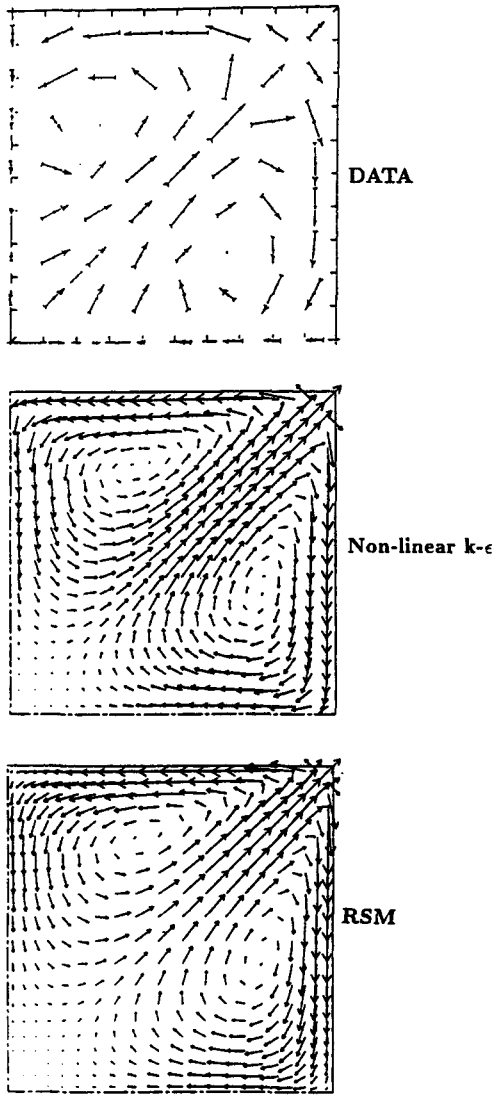

Figure 2. Secondary-velocity vectors.
Data of Brundrett and Baines (1964).

PREDICTIONS: ——— Non-linear k-ε
..... RSM

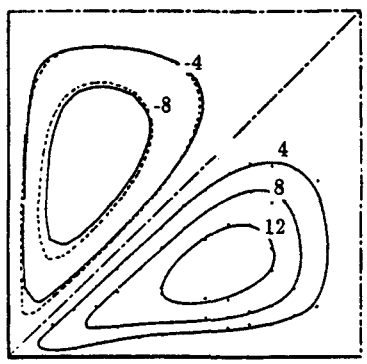

DATA

Figure 3. Secondary flow streamlines $\Psi \times 10^4$.
Data of Gessner and Jones (1965).

PREDICTIONS: ——— Non-linear k-ε
..... RSM

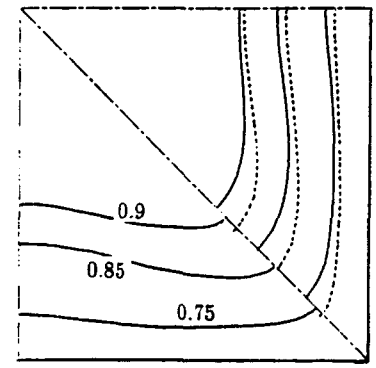

DATA

Figure 4. Mean velocity contours W/W_{max}.
Data of Brundrett and Baines (1964).

the wall bisector, and outwards toward the corners, a behavior that is only qualitatively reproduced by either model. Turning now to the turbulence field, Figure 5 compares the predicted and measured component of normal-stress anisotropy that contributes directly to the generation of streamwise vorticity [plotted as $(\overline{u^2}-\overline{v^2})/W_\tau^2$, where W_τ is the friction velocity]. It is immediately clear that the two models yield close results for this parameter over most of the flow domain. And, although the Reynolds-stress model results are in better overall agreement with the data, it is encouraging to note that the $k-\epsilon$ model results appear to correctly reproduce the overall levels of turbulence kinetic energy and the proportions in which this quantity is partitioned among its components (had the linear relation been used, then the predicted normal-stress anisotropy would have been zero everywhere). The gradients of the shear-stress component $\overline{vw}$ act to diffuse the streamwise velocity in the y-direction, and the present results for this quantity are compared with the data of Gessner and Po (1976) in Figure 6. Here again the two models yield essentially identical results that tend to agree well with the data, especially away from the wall.

Leutheusser (1963) obtained measurements in a rectangular duct of aspect ratio 3 at $Re = 5.6\times10^4$, and these are used now to check the models. Here, again, only one-quarter of the complete cross section was computed, on a grid of

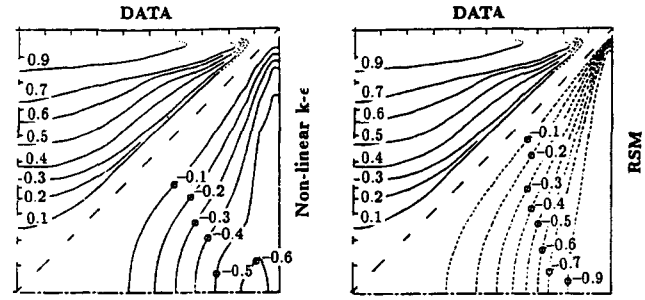

Figure 5. Normal stress anisotropy contours $(\overline{u^2}-\overline{v^2})/W_\tau^2$.
Data of Brundrett and Baines (1964).

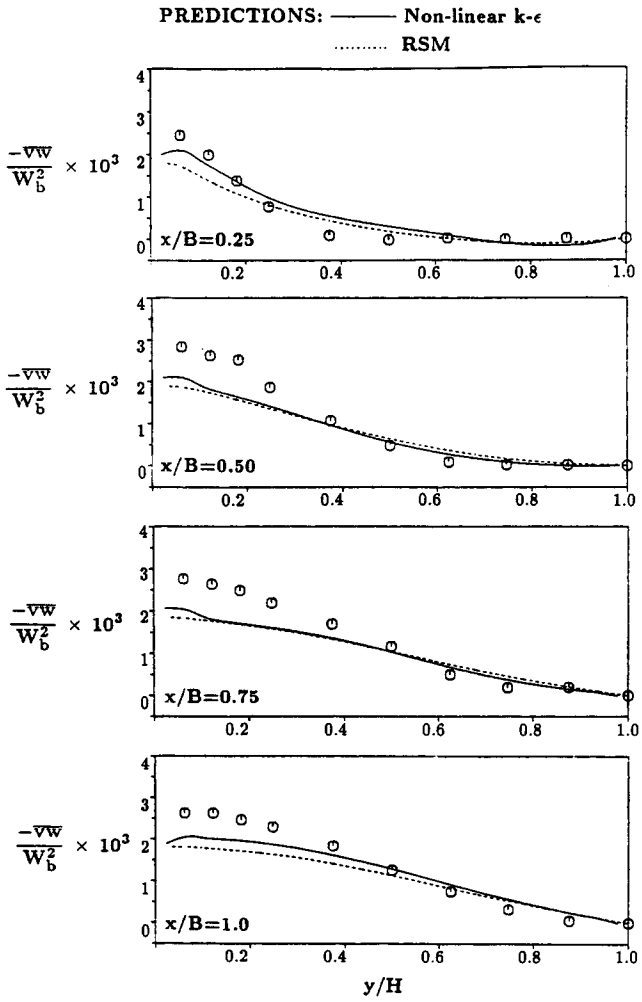

Figure 6. Main-shear-stress profiles.

Data of Gessner and Po (1976).

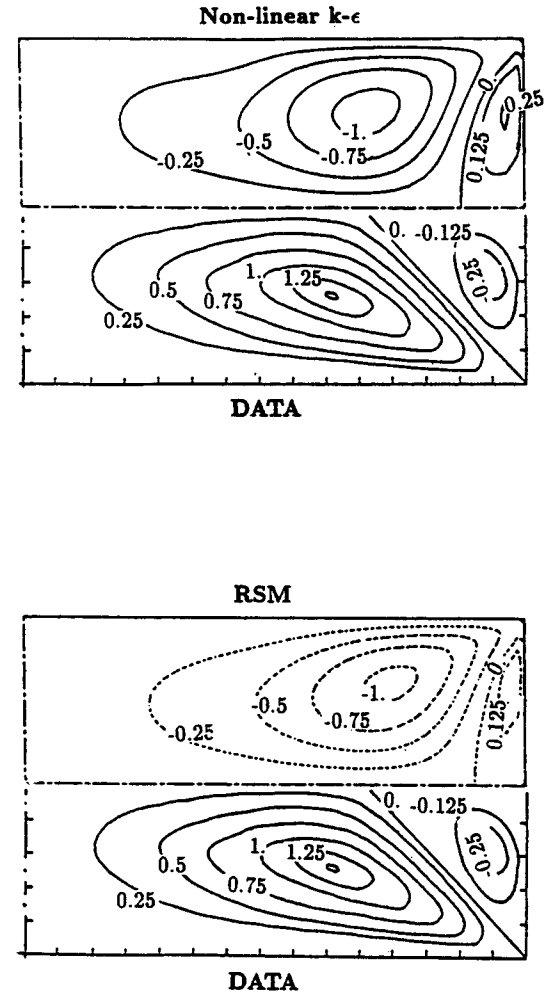

Figure 7. Secondary-velocity streamlines $\Psi \times 10^3$.

Data of Hoagland (1960).

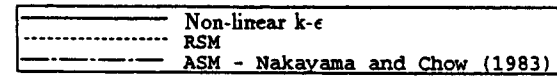

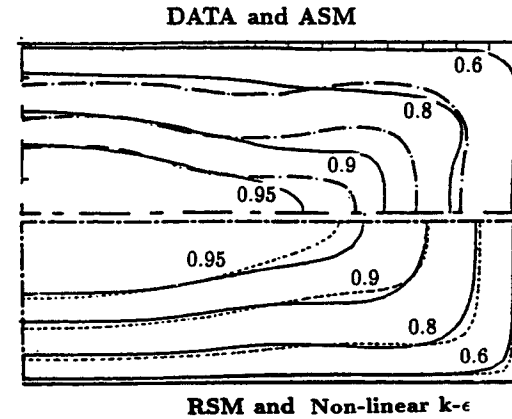

Figure 8. Mean-velocity contours W/W_{max}.

Data of Leutheusser (1963).

42×22 nodes. The predicted and measured contours of the secondary-velocity streamlines are compared in Figure 7 while the corresponding contours of the main velocity (normalized by $\overline{W}$) are presented in Figure 8, which also shows the Algebraic Model Results of Nakayama et al. (1983). A similar distortion to the main velocity profiles to that in the square duct is observed, and this is produced marginally better with the Reynolds-stress closure. There is some hint then that the nonlinear model is not capturing the turbulence anisotropy particularly well in this case, and this is confirmed from Figure 9, which compares this parameter with the measurements of Hoagland (1960) in a duct with an aspect ratio of 3 but with $Re = 2 \times 10^4$. Clearly, the model underestimates the magnitude of turbulence anisotropy but this is not altogether surprising, since the transport effects make some contribution to the turbulence anisotropy, and these effects are entirely absent from the nonlinear eddy-viscosity model.

One consequence of turbulence-driven secondary motions with important practical implications is the change they bring about in the magnitude and distribution of the shear stresses at the wall. Figure 10 compares the present predictions of this parameter with the data of Knight and Patel (1985) for eight ducts with aspect ratio varied in the range 1–6.25. For the small ratio ducts, there is a marked shift in the position

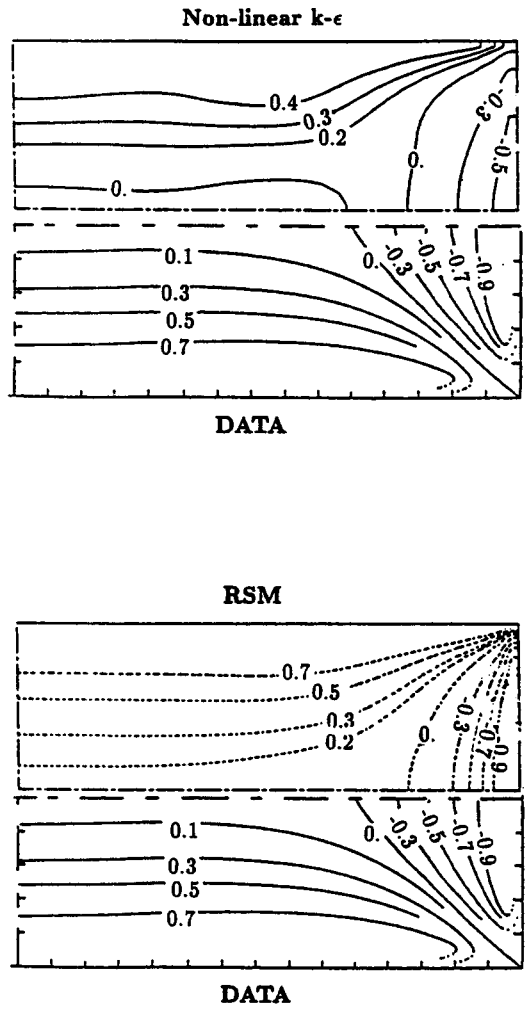

Figure 9. Normal-stress-anisotropy contours $(\overline{u^2}-\overline{v^2})/W_\tau^2$.

Data of Hoagland (1960).

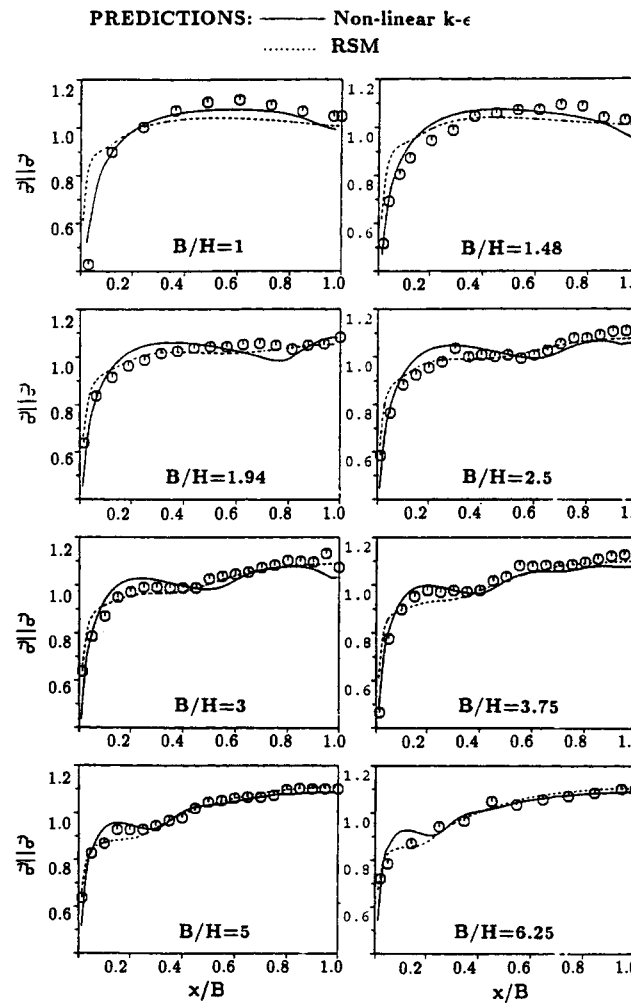

Figure 10. Bed shear stress for rectangular ducts.

Data of Knight and Patel (1985).

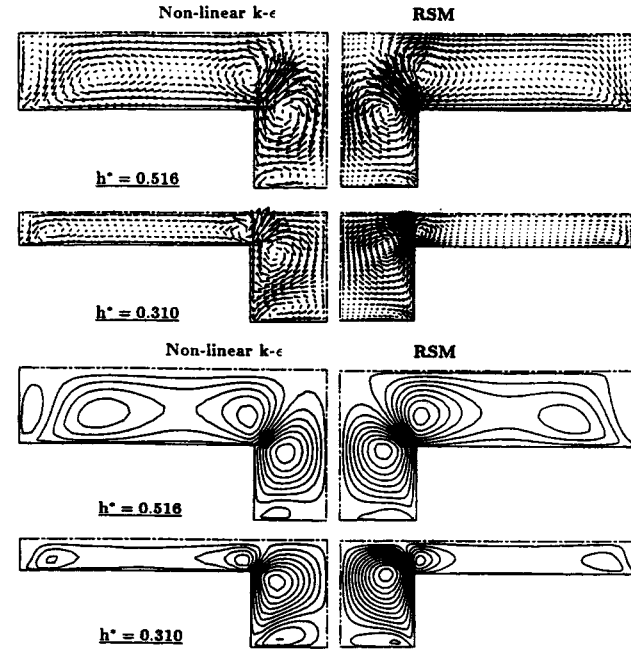

Figure 11. Secondary-velocity vectors in compound symmetric ducts.

of maximum shear stress away from the center line (where it would occur in two-dimensional flow) and toward the corners. A region of "stress-deficit" is thus created, and this is seen to migrate toward the corner with increasing aspect ratio. The extent of this deficit, and its rate of migration, are predicted fairly accurately by both models.

Attention is now turned to flows in compound ducts formed from a combination of a deep main duct and shallower side ones. Figure 11 shows the present results for the two values of the depth ratio h^* of 0.31 and 0.516. Plotted there are the secondary-flow vectors and streamlines, and these clearly show the formation of a "fountain effect" along the diagonal of the internal step, formed from the interaction between secondary cells formed in the main and side ducts. Knight and Lai (1985) reported measurements of the contours of streamwise velocity, and these are shown in Figure 12, where the present predictions are also plotted. The distortion wrought by the secondary-flow cells is clear: a severe deflection along the step diagonal leading, for the $h^* = 0.516$ case, to the formation of two separate maximum velocity streams: one along the center line of the main duct, and the other at approximately a third of the side-duct width. Both models

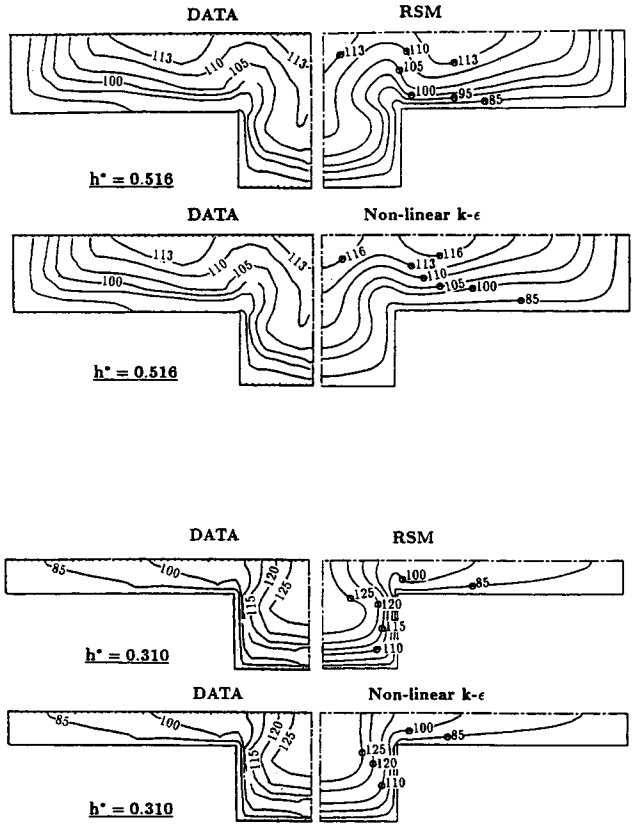

Figure 12. Mean-velocity contours $W/W_b \times 10^2$.

Data of Knight and Lai (1985).

reproduce this feature quite well. The predicted and measured wall shear-stress distributions are shown in Figure 13. On the side-duct walls, the measurements for this quantity show a marked depression around $x/B = 0.4$, and this is somewhat better predicted by the nonlinear model. Both models appear to reproduce, fairly well, the reduction in wall shear stress on the main duct wall with the approach to the side duct, and the sudden rise in shear stress there.

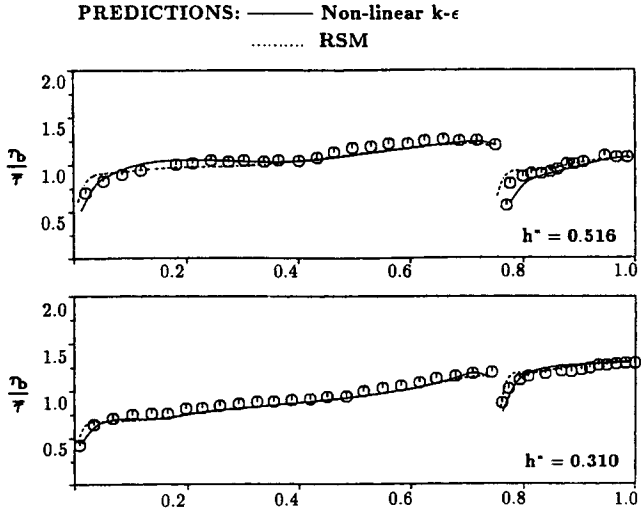

Figure 13. Bed shear stress in compound ducts.

Data of Knight and Lai (1985).

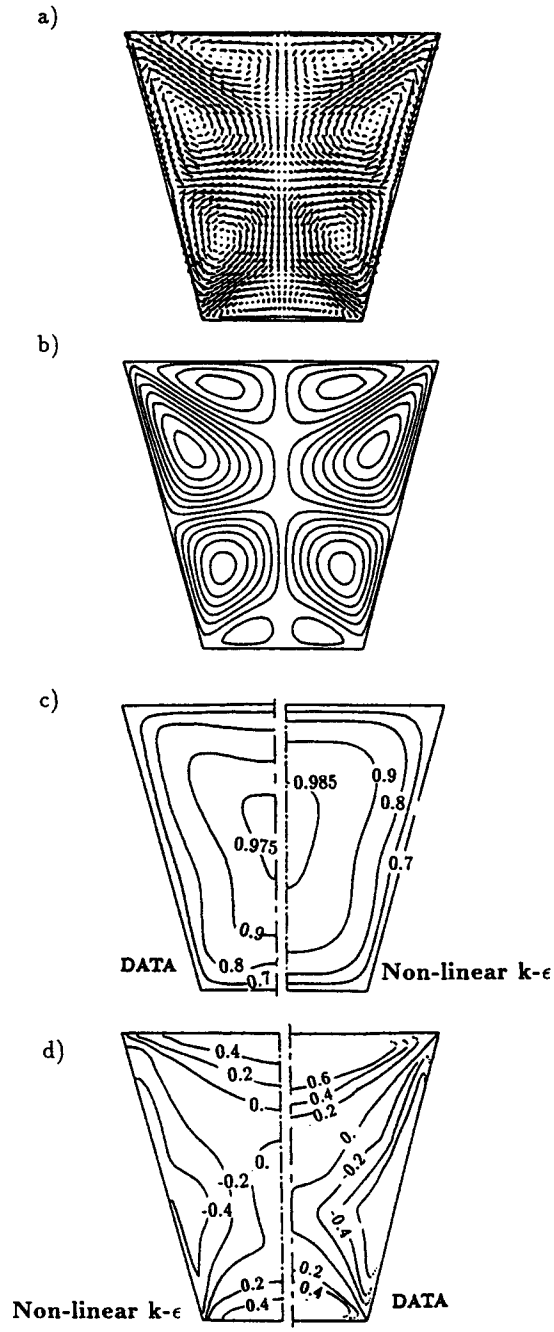

Figure 14. Nonlinear k-ϵ model results.

(a) Secondary-velocity vectors; (b) secondary-velocity streamlines; (c) mean-velocity contours W/W_{max}; (d) turbulence anisotropy $(\overline{u^2} - \overline{v^2})/\overline{W_\tau}^2$ (data of Rodet, 1960).

Data from flows in trapezoidal ducts provide another check on the nonlinear model performance. Measurements have been reported by Rodet (1960) for $Re = 2.4 \times 10^5$ and $AR = 0.82$. The present predictions (obtained on a grid of 34×42) are presented in Figure 14. The model reveals the existence of an exotic system of secondary-flow cells leading to main-flow distortion which compares quite well with the measurements. The turbulence anisotropy is somewhat better predicted than before, an unexpected outcome in view of the additional complexity wrought by asymmetry.

Conclusions

A two-equation $k - \epsilon$ model of turbulence, used in combination with Speziale's nonlinear stress-strain relationship, and a complete Reynolds-stress transport closure were used to predict the behavior of turbulent flows in some representative ducts of noncircular cross sections. It was found that both models capture, to acceptable engineering accuracy, the main features of these flows, namely the emergence of secondary-flow cells that are driven by the turbulence anisotropy and that lead to the distortion of the streamwise velocity distribution. Moreover, both models also reproduce fairly well the displacement of the location of maximum wall shear stress toward the corners in the small aspect-ratio ducts. Implementation of the nonlinear model in a staggered-grid code does not pose special difficulties, and this, coupled with the observation that its performance is comparable to that of the Reynolds-stress closure but at much less cost, recommends it for serious consideration for use in routine engineering calculations.

Acknowledgment

This work was supported by the U.K. Engineering and Physical Sciences Research Council under grant GR/H45636.

Notation

AR = aspect ratio of the duct
B = half width of duct
b = half width of main part of duct
C_1, C_1', C_2, C_2' = Reynolds-stress model coefficients
$C_{\epsilon 1}, C_{\epsilon 2}, C_\mu, C_f$ = turbulence model coefficients
f_x, f_y = damping functions
h = height of flood plain
H = depth of main duct
n_i = unit vector normal to the surface
p, p' = time-averaged and fluctuating values of pressure
P_k = production of turbulent kinetic energy
u, v, w = fluctuating velocity components in x-, y- and z-directions
W_τ = friction velocity
$\overline{u^2}, \overline{v^2}, \overline{w^2}$ = normal-stress components
x, y, z = spanwise, normal, and streamwise coordinate direction
δ_{ij} = Kronecker delta
κ = von Karman constant
ν = molecular kinematic viscosity
ρ = density
Ψ = secondary flow stream function
σ_ϵ = coefficient of turbulent diffusion of ϵ
$\bar{\tau}$ = average shear stress

Subscripts

b = bed
t = turbulent
w = wall

Literature Cited

Brundrett, E., and W. D. Baines, "Production and Diffusion of Vorticity in duct flow," *J. Fluid Mech.*, **19**, 375 (1964).

Daly, B. J., and F. H. Harlow, "Transport equations in turbulence," *Phys. Fluids*, **13**, 2634 (1970).

Demuren, A. O., and W. Rodi, "Calculation of Turbulence Driven Secondary Motion in Non-circular Ducts," *J. Fluid Mech.*, **140**, 189 (1984).

Gessner, F. B., and J. B. Jones, "On Some Aspects of Fully Developed Turbulent Flow in Rectangular Channels," *J. Fluid Mech.*, **23**, 689 (1965).

Gessner, F. B., and J. K. Po, "A Reynolds Stress Model for Turbulent Corner Flows: II. Comparisons Between Theory and Experiment," *J. Fluids Eng.*, **98**, 269 (1976).

Gibson, M. M., and B. E. Launder, "Ground Effects on Pressure Fluctuations in the Atmospheric Boundary Layer," *J. Fluid Mech.*, **86**, 491 (1978).

Hoagland, L. C., "Fully Developed Turbulent Flow in Straight Rectangular Ducts," PhD Thesis, M.I.T, Cambridge, MA (1960).

Knight, D. W., and C. J. Lai, "Turbulent Flow in Compound Channels and Ducts," Int. Symp. on Refined Flow Modeling and Turbulence Measurements, Iowa City, IA (1985).

Knight, D. W. and H. S. Patel, "Boundary Shear Stress in Smooth Rectangular Ducts," *J. Hydraul. Eng.*, **111**, 29 (1985).

Launder, B. E., G. J. Reece, and W. Rodi, "Progress in the Development of a Reynolds Stress Turbulence Closure," *J. Fluid Mech.*, 68, 537 (1975).

Leutheusser, H. J., "Turbulent Flow in Rectangular Ducts," *J. Hydraul. Div., ASCE*, **89** (HY3), 1 (1963).

Lumley, J. L., "Toward a Turbulent Constitutive Relation," *J. Fluid Mech.*, **41**, 413 (1970).

Nakayama, A., W. Chow, and D. Sharma, "Calculation of Fully Developed Turbulent Flows in Ducts of Arbitrary Cross-section," *J. Fluid Mech.*, **128**, 199 (1983).

Patankar, S. V., "Numerical Heat Transfer and Fluid Flow," McGraw-Hill, New York (1980).

Patankar, S. V., and D. B. Spalding, "A Calculation Procedure for Heat, Mass and Momentum Transfer in Three-Dimensional Parabolic Flows," *Int. J. Heat Mass Transfer*, **15**, 1787 (1972).

Pope, S. B., "A More General Effective-Viscosity Hypothesis," *J. Fluid Mech.*, **72**, 331 (1975).

Rodet, E., "Etude de l'ecoulement d'un fluide dans un tunnel prismatique de section trapezoidale," Publ. Sci. Technol. Min. l'Air, No. 369 (1960).

Rotta, J., "Statistical Theory of Non-homogeneous Turbulence," *Z. Phys.*, **129**, 547 (1951).

Shir, C. C., "A Preliminary Study of Atmospheric Turbulent Flow in the Idealized Planetary Boundary Layer," *J. Atmos. Sci.*, **30**, 1327 (1973).

Speziale, C. G., "On Nonlinear k-l and k-ϵ Models of Turbulence," *J. Fluid Mech.*, **178**, 459 (1987).

Younis, B. A. and O. E. Abdellatif, "Modeling of Sediment Transport in Rectangular Ducts with a Two-equation Model of Turbulence," *Proc. Int. Symp. on Sediment Transport Modeling*, ASCE, New Orleans, LA, 197 (1989).

Younis, B. A., "Boundary Layer Calculations with Reynolds Stress Turbulence Models," Mechanical Engineering Department Report FS/82/25, Imperial College, London (1982).

Younis, B. A., "On Modeling the Effects of Streamline Curvature on Turbulent Shear Flows," PhD Thesis, Imperial College, London, (1984).

Manuscript received May 13, 1996, and revision received Nov. 18, 1996.